Samimi, M., Wang, K., Azar, Y., Wong, G. N., Mayzus, R., Zhao, H., Schulz, J. K., Sun, S., Gutierrez, F., Rappaport, T. S., "28 GHz Angle of Arrival and Angle of Departure Analysis for Outdoor Cellular Communications using Steerable Beam Antennas in New York City," to appear in the 2013 IEEE Vehicular Technology Conference (VTC), June 2~5, 2013.

28 GHz Angle of Arrival and Angle of Departure Analysis for Outdoor Cellular Communications using Steerable Beam Antennas in New York City

Mathew Samimi, Kevin Wang, Yaniv Azar, George N. Wong, Rimma Mayzus, Hang Zhao,
Jocelyn K. Schulz, Shu Sun, Felix Gutierrez, Jr., and Theodore S. Rappaport
NYU WIRELESS Center
Polytechnic Institute of New York University, Brooklyn, NY 11201
tsr@nyu.edu

***Abstract*— Propagation measurements at 28 GHz were conducted in outdoor urban environments in New York City using four different transmitter locations and 83 receiver locations with distances of up to 500 m. A 400 mega-chip per second channel sounder with steerable 24.5 dBi horn antennas at the transmitter and receiver was used to measure the angular distributions of received multipath power over a wide range of propagation distances and urban settings. Measurements were also made to study the small-scale fading of closely-spaced power delay profiles recorded at half-wavelength (5.35 mm) increments along a small-scale linear track (10 wavelengths, or 107 mm) at two different receiver locations. Our measurements indicate that power levels for small-scale fading do not significantly fluctuate from the mean power level at a fixed angle of arrival. We propose here a new lobe modeling technique that can be used to create a statistical channel model for lobe path loss and shadow fading, and we provide many model statistics as a function of transmitter-receiver separation distance. Our work shows that New York City is a multipath-rich environment when using highly directional steerable horn antennas, and that an average of 2.5 signal lobes exists at any receiver location, where each lobe has an average total angle spread of 40.3° and an RMS angle spread of 7.8°. This work aims to create a 28 GHz statistical spatial channel model for future 5G cellular networks.**

Keywords—28 GHz, 5G, millimeter wave, RF propagation, channel sounder, statistical spatial channel model, AOA, AOD, lobe, angle spread, path loss, shadow fading, polar plot.

I. INTRODUCTION

Recent work has suggested the viability of mm-wave spectrum (i.e. at 28 GHz and 38 GHz) to satisfy the increased bandwidth demand for cellular and backhaul; these bands provide much more spectrum and allow the use of miniature high gain antennas [1][2][3]. Fig. 1 shows the relationship between atmospheric attenuation at sea level and frequency. The additional propagation attenuation at 28 GHz is about 0.06 dB/km; however, since the maximum cell size is projected to be 200 m at 28 GHz [4], the vertical axis of Fig. 1 can be divided (in dB) by a factor of five. Thus, atmospheric attenuation is 0.012 dB/200 m at 28 GHz, a negligible value like cellular bands used today. When using directional antennas, urban propagation and rain attenuation are also not major concerns at 28 GHz [4].

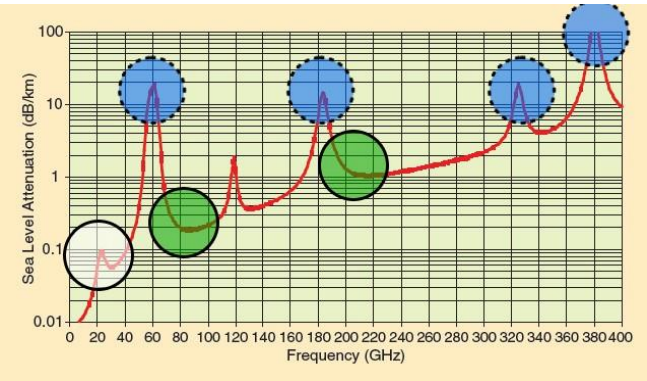

Fig. 1. Air attenuation at sea level versus frequency, showing the additional path loss due to atmospheric oxygen [2]. The white circle highlights the 28 GHz and 38 GHz frequency bands that will be used for future 5G wireless. The green circles (solid border) highlight frequencies that have comparable free space (air) characteristics to modern cellular frequencies. The blue circles (dotted border) show frequencies with greater attenuation, which are therefore ideal for short-range indoor communications.

Using the mm-wave spectrum for future cellular and backhaul networks will not only alleviate the current spectrum shortage, but also offer multi-gigabit per second data for each mobile user. Recent analysis has shown that the relative power consumption of wireless devices decreases as the RF bandwidth increases [5], implying that future smartphones will not only have faster data rates, but also be more energy efficient.

The commercialization of mm-wave cellular can be realized with high-gain steerable antennas, which are necessary to overcome the propagation challenges of higher carrier frequencies, and to direct energy towards optimal directions that can exploit multipath and successfully complete a link [6]. Future smart antenna arrays, possibly on-chip [1], will algorithmically determine the optimal angle of arrival (AOA) and angle of departure (AOD). One possible beam steering method is to use narrowband pilot tones that enable the prediction of the spatial location of multipath based on narrowband

envelope cross-correlations [7].

The study of indoor spatial propagation of multipath has been investigated in the past, as multipath AOA was determined in a classroom, hallway, and parking lot using highly directional antennas and ray-tracing techniques [8]. In [8], the azimuthal multipath distribution was found to be highly correlated with the site-specific environment.

A common misconception about mm-wave propagation is that a link can only be completed between a TX and a RX in a line of sight (LOS) environment. Previous outdoor propagation research in Brooklyn, NY for local multipoint distribution service (LMDS) at 28 GHz demonstrated that LOS links work well, but non line of sight (NLOS) links do not [11]. Recent studies of the 38 GHz and 60 GHz mm-wave channels conducted at the University of Texas [12] concluded that making links was rare at extreme off-boresight angles (i.e. with the receiver antenna pointed 50° or more away from the optical unobstructed LOS direction to the TX). However, in this 28 GHz study, we see that in downtown New York City, making links at off-boresight pointing angles is not only possible, but very common.

II. 28 GHz Broadband Channel Sounder Hardware and Measurement Procedure

This measurement campaign was conducted around the Polytechnic Institute of New York University (NYU-Poly) campus in downtown Brooklyn, and the NYU main campus in Manhattan. The Brooklyn TX was located on the rooftop of Rogers Hall (eight stories high, 40 m above ground level) with eight RX locations, where two NLOS locations were chosen specifically to investigate small-scale fading. The three Manhattan TX sites were chosen to emulate future cellular base stations with relatively low heights: two were located on the one-story Coles Sports Center building rooftop (7 m above ground level, with the TX located on the northwest and northeast corners of the roof), and one TX was located on the five-story balcony of the Kaufman building of the Stern Business School (17 m above ground level, see Fig. 3). All three Manhattan TX sites used the same set of 25 RX locations, which were chosen randomly based on the availability of AC power, thus yielding 75 unique TX-RX locations in Manhattan and 83 in total including Brooklyn. Multipath power delay profiles as a function of TX and RX beam steering directions were recorded at each RX location for which signal could be received (28 RX locations in Manhattan). At each RX location, the narrow beam (10° beamwidth) horn antennas for both the TX and RX antennas were first rotated to find the strongest received power. The 0° azimuth angles of the TX and RX antennas were specified as the TX and RX pointing angles that provided the strongest signal at the RX. Then, nine different azimuth/elevation pointing combinations were used, and complete 360° azimuthal scans of the RX antenna were conducted in 10° increments

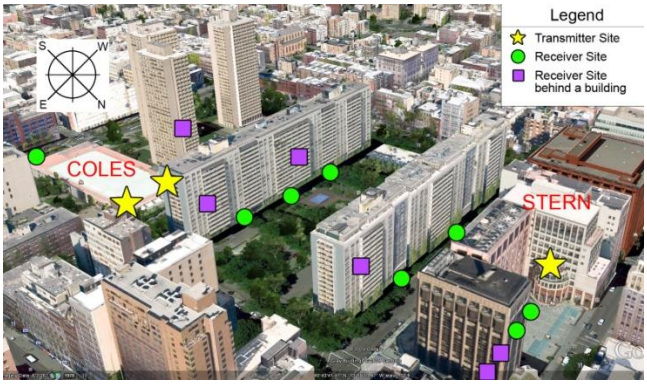

Fig. 3. 28 GHz cellular measurement locations in Manhattan near the NYU campus. Three base station locations (yellow stars on the one-story rooftop of Coles Recreational Center and five-story balcony of the Kaufman building of Stern Business School) were used to transmit to each of the 25 RX locations within 20 to 500 m. Green dots represent visible RX locations, and purple squares represent RX sites that are blocked by buildings in this image. Four RX locations on the west are not shown in the picture (including the eight RX sites in Brooklyn).

to capture PDPs. PDP measurements were taken for three different TX azimuth angles, -5°, 0°, and +5° using a fixed TX antenna downtilt of -10°, and for three different RX elevations, -20°, 0°, and + 20. A 10th antenna combination allowed us to measure AOD statistics, where the RX was pointed in elevation and azimuth for strongest received signal, and the TX was then swept in azimuth in 10° increments using a fixed downtilt of -10°. For each TX-RX antenna pointing combination at each RX location, we measured PDPs using a 400 mega-chips per second spread spectrum sliding correlator channel sounder with a slide factor of 8000, a multipath resolution of 2.3 ns, and a RF null-to-null bandwidth of 800 MHz [4]. The TX and RX antennas were mechanically auto-steered in 10° increments over azimuth using vertically polarized 24.5 dBi horn antennas (3-dB beamwidth of 10.9°). Accounting for a SNR of 10 dB, the maximum measurable path loss was 168 dB, with a transmit power of +30 dBm applied to the TX antenna [4].

Using LabVIEW software provided by National Instruments, an average PDP was measured at each TX-RX pointing angle combination at each RX location, for each 10° increment in azimuth at the RX, enabling spatial and temporal multipath statistics to be computed, where each average PDP was made up of 20 successive $I^2 + Q^2$ PDPs recorded over a four second interval.

Small-scale linear track measurements were first conducted in Brooklyn (Figs. 4 and 6) with a step size of 5.35 mm ($\lambda/2$) along a 107 mm (10λ) length track. The RX azimuth angle was set to 0° when the RX antenna pointed directly at the TX, for LOS and NLOS conditions. At each λ/2 track position, measurements were recorded at 10° counterclockwise azimuth increments at the RX to perform a 360° sweep with the TX azimuth held constant. Thus, 36 PDP measurements were completed at each λ/2 position for small-scale fading analysis.

Since relatively little fading was observed for each multipath component over the linear track, AOA and AOD

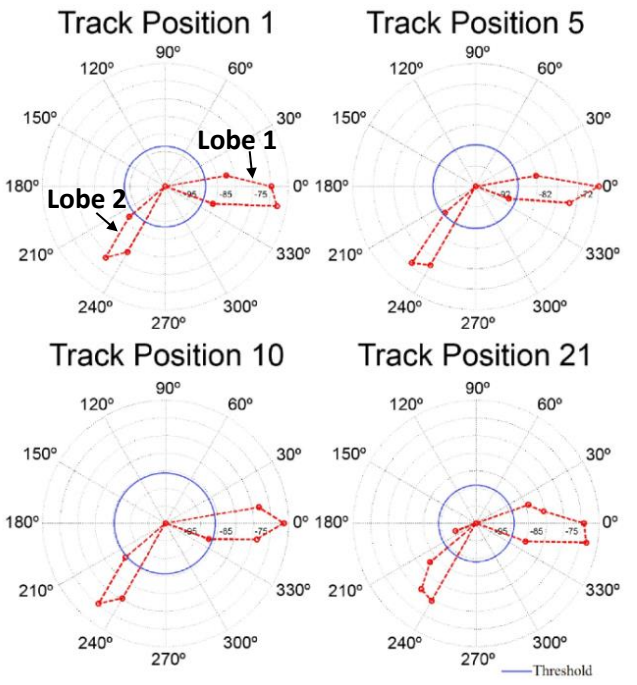

Fig. 4. Four polar plots of 28 GHz propagation at track positions 1, 5, 10 and 21 along a 21-step linear track with λ/2 step sizes show two lobes of received power across azimuth. Measurements are for a partially obstructed NLOS RX environment in downtown Brooklyn using 24.5 dBi horn antennas at both the TX and RX. The TX was placed on the rooftop of NYU-Poly's Rogers Hall 135 m away from the RX. Each red dot represents the received power level at a particular RX azimuth angle. For NLOS RX locations, a threshold of 20 dB below maximum power level was defined for a threshold (shown as a blue solid-line circle) to determine lobe statistics. 10 dB was used for LOS.

measurements were conducted in Manhattan without the linear track.

III. 28 GHz Channel AOA and AOD Analysis Using Lobes

Multipath power delay profiles were captured at each RX and TX angular orientation, providing received PDPs and multipath statistics as a function of azimuth angle at both TX and RX. The received power is the area under the PDP and may be plotted on polar plots, as shown in Fig. 4. We define a *lobe* as the contiguous spread of energy arriving or departing in the azimuth and elevation directions, where each distinct lobe defines a principal propagation route (e.g. spatial direction) of multipath. Lobes are 3-D in general, but in this paper, we show lobes as 2-D representations of azimuthal power distribution, which may represent either AOA (arriving at RX) or AOD (departing from TX).

Fig. 4 shows an example of received power (PDP) measurements taken in a NLOS environment with the TX on the rooftop of Rogers Hall and the RX at the corner of Bridge Street and Myrtle Avenue in downtown Brooklyn, over a small-scale 10 wavelength, 21 position track of 107 mm in length, where each incremental position is separated by 5.35 mm. The TX-RX separation distance was 133 m. Fig. 4 shows energy arriving at the RX (e.g. AOA) over a small-scale local area from two distinct directions (e.g. two distinct lobes), where each of the two lobes has varying angle spread and power intensity. Table 1 lists several statistics we have defined in order to model lobes consistently. We define $\bar{\theta}$ as the AOA (at the RX) or AOD (at the TX) for a particular lobe, where $\bar{\theta}$ represents the power-weighted mean pointing angle. We use $\bar{\theta}$ of each lobe to identify the single (e.g. mean) direction of energy arrival or departure calculated by (1),

$$\bar{\theta} = \frac{\sum_k P(\theta_k)\theta_k}{\sum_k P(\theta_k)} \quad (1)$$

where k is the index of a pointing angle θ_k (degrees) within a lobe and $P(\theta_k)$ is the received power (in the linear scale, e.g. mW) at θ_k.

Lobes 1 and 2 in Fig. 4 have an approximate "visual" AOA of 0° and 230° at all track positions. However, using (1), Lobes 1 and 2 at track position 1 have a precise AOA of

TABLE 1: SUMMARY OF LOBE STATISTICS, THE PROCEDURE TO COMPUTE THEM, THEIR PHYSICAL MEANING, AND THE EMPIRICAL DISTRIBUTIONS FOR ALL MANHATTAN RX LOCATIONS.

Statistics	***Computation Procedure***	***Physical Meaning***	***Empirical Distribution in Manhattan***
AOA	$\bar{\theta} = \frac{\sum_k P(\theta_k)\theta_k}{\sum_k P(\theta_k)}$	The mean direction of arrival of a lobe	Uniform [0°, 360°]
Lobe angle spread (LAS)	Apply threshold to polar plot, e.g., 10 dB of peak at LOS RX location, 20 dB for NLOS	Angle span of a lobe above a pre-defined threshold	Exponential μ = 40.3° σ = 42.5°
RMS LAS (standard deviation of lobe angle spread)	RMS LAS = $\sqrt{\overline{\theta^2} - (\bar{\theta})^2}$ where $\overline{\theta^2} = \frac{\sum_k P(\theta_k)\theta_k{}^2}{\sum_k P(\theta_k)}$	Angle span of lobe in which most power is received	Exponential μ = 7.8° σ = 10.7°
# of lobes for a particular RX location/antenna configuration	Number of lobes above pre-defined threshold	# of spatial directions from TX to RX	Exponential μ = 2.5 σ = 1.7
Total power in a lobe for a particular RX location/antenna configuration	$\sum_k P(\theta_k)$ over consecutive k values where $P(\theta_k)$ above threshold	Total power in a lobe	Applies to each lobe at each RX for a particular antenna configuration at TX and RX
Average power in lobe for a particular RX location/antenna configuration	$\frac{\sum_k P(\theta_k)}{k_{max}}$ over consecutive k values where $P(\theta_k)$ above threshold	Average power in a lobe	Applies to each lobe at each RX for a particular antenna configuration at TX and RX
Max power in a lobe for a particular RX location/antenna configuration	$\max_k P(\theta_k)$ over consecutive k values where $P(\theta_k)$ above threshold	Max power in a lobe.	Applies to each lobe at each RX for a particular antenna configuration at TX and RX

354.4° and 235.6°, respectively.

As shown in Table 1, we define a lobe as a shape on a polar plot of received signal (e.g. multipath) power, wherein each lobe has statistics such the *lobe angle spread* (LAS) (the span of RX or TX azimuth angles over which the lobe has energy and thus exists), and the root mean square deviation (RMS) of LAS (which denotes the angle spread across azimuth of a lobe over which *most* of the total lobe power is received). These statistics and their computation methods are given in Table 1, including the particular values of these statistics for the set of all lobes measured at all Manhattan locations that had sufficient signal strength (at 6 LOS and 22 NLOS RX locations). The measured data revealed the average and standard deviation of the number of lobes found in all Manhattan measurements was 2.5 and 1.7, respectively, and can be well modeled as an exponential random variable about the mean (2.5) number of lobes. The average and standard deviation of the LAS (defined in Table 1) for all Manhattan locations that could be measured was 40.3° and 42.5° respectively, and is well modeled as an exponential random variable about the mean. The AOA $\bar{\theta}$ over all Manhattan locations was found to perfectly match a uniform distribution between 0° and 360°.

The azimuthal distributions of multipath signals as described by spatial lobes is one important part of a proper *statistical spatial channel model* (SSCM) for cellular communications at 28 GHz, but it is also important to model the propagation in the time domain (e.g. multipath propagation in time) [9][10]. We define a *multipath cluster* as a group of multipath components within a PDP for a particular RX and TX antenna spatial angle such that a cluster represents *signal energy travelling closely together in time and angular space*. Note that for channel modeling purposes, the beam pointing angle may be defined simply as a lobe (e.g. the RMS LAS about the AOA), or as a sampled portion of a lobe about the AOA, or may be defined in terms of the RX antenna pattern (e.g. beamwidth) and its orientation. An important statistic for a PDP is the number of clusters in a PDP. A cluster is defined by its initial arrival time, that is, the propagation time of the first arriving multipath component within a cluster, the cluster time spread, the cluster internal RMS delay spread, the multipath amplitude distribution of the cluster, the number of multipath components contained within each cluster, and the inter-arrival time distributions of multipath components within a cluster. We can also statistically model void arrival times, (e.g. time intervals between two consecutive clusters in a PDP). Finally, we define a *path* as the strongest multipath component within each cluster. A path is defined by its amplitude, and its excess or absolute propagation time delay within the cluster. Table 2 summarizes the above definitions.

Fig. 5a shows the relative propagation times of the power received at Angle 1 of 350° and Angle 2 of 230° (e.g. Lobes 1 and 2, respectively) of the polar plot in Fig. 4 at Track Position 1, corresponding to the PDPs with the

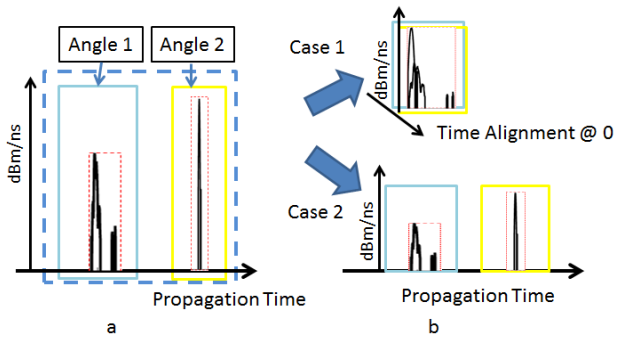

Fig. 5 a) Superimposed PDP of two individual received PDPs, where each PDP comes from a different AOA at the same RX location. The PDPs displayed are from the polar plot in Fig. 4 at a partially obstructed NLOS environment RX in downtown Brooklyn at Track Position 1 at 28 GHz, shifted in time according to their absolute propagation times. The multipath signals from Angle 1 arrived before those of Angle 2 (i.e. multipath arriving at different times from two distinct lobes). The absolute propagation times were found using manual ray-tracing, thus allowing alignment with absolute timing of multipath signals at the RX, independent of AOAs. b) Case 1 illustrates a situation where the receiver is not able to recover absolute propagation times of arrival, resulting in all PDPs aligned to the same point (first arriving multipath) in time. Case 2 illustrates a situation where the receiver is able to distinguish absolute propagation times across azimuth, thus keeping track of the absolute temporal distribution of received power.

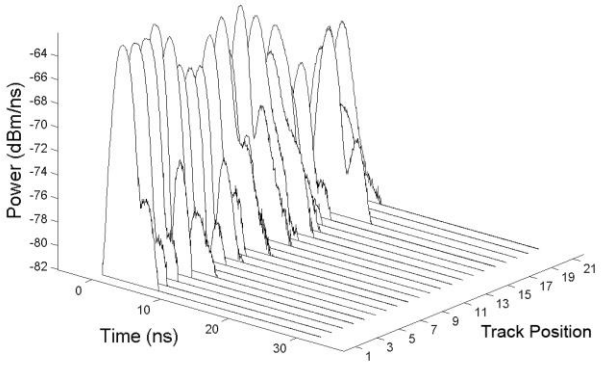

Fig. 6. PDPs measured over a 10λ linear track. The TX was on the rooftop of Rogers Hall in downtown Brooklyn, and the RX was on Bridge Street (135 m away from the TX). The TX and RX were pointed for maximum signal power. Track step size was λ/2 using 24.5 dBi horn antennas with 3-dB beamwidth of 10.9°.

greatest received power within the lobes. Since our measurement system sequentially measured multipath over 10° azimuth increments and did non-coherent detection, we did not have absolute propagation time delays for each arriving PDP, as the first arriving multipath component was used to trigger and establish the relative time delay as zero for all PDPs. This limitation is illustrated as Case 1 in Fig. 5, where we have used ray in conjunction with city 3-D maps to synthesize absolute propagation times of the strongest multipath PDPs to yield the desired Case 2 [4]. Future measurements using cesium clock standards and synchronization will ensure true propagation times for all PDPs, removing the need to synthesize absolute propagation times with ray-tracing. Case 2 shows the desired situation where the receiver distinguishes the absolute time delays of

TABLE 2: SUMMARY OF TEMPORAL CHANNEL MODEL STATISTICS AND DEFINITIONS.

Terminology	Definition	Statistics
Cluster	Group of multipath components within a PDP traveling closely in propagation time delay at a specified lobe or direction in space	1. Cluster time duration 2. Internal RMS delay spread 3. Multipath amplitude distribution 4. Inter-arrival distributions of multipath within cluster 5. Number of multipath components within the cluster 6. Number of clusters in a PDP for a specified lobe or direction in space
Void	Time interval between two consecutive clusters	1. Void duration 2. Number of voids in a PDP
Path	The strongest multipath component within a cluster	1. Excess time delay 2. Amplitude
Sub-path	Individual multipath component	1. Excess time delay 2. Amplitude

all arriving multipath at all angles, enabling completely accurate characterization of both angular and temporal statistics of the wireless channel that may be used for any type of antenna or beamforming/MIMO analysis (e.g. an omni-directional channel model) [4].

Fig. 6 shows small-scale PDP measurements in a NLOS location. For the strongest, first arriving multipath component, the maximum instantaneous received power along the track was -64 dBm/ns, while the minimum was -68 dBm/ns, demonstrating little fading with a ± 2 dB fluctuation about the mean power level at a given AOA. As shown in Figs. 4 and 6, the small scale fading is negligible over 10λ distance and constant AOA, suggesting that developers of future wideband modems can expect little fading within small-scale movements of 10 wavelengths (0.107 m). With beam-steering and MIMO techniques, antennas will be pointed over azimuth and elevation angles to exploit the strongest powers.

Most links between TX and RX occured within ± 100° for the TX azimuth, accounting for 91.6% of the total number of viable links of 168 dB path loss or less, and within ± 160° for the RX azimuth, accounting for 90.6% of the total number of links. These show that there are micro-cellular urban environments such as Manhattan that offer many viable combinations of TX-RX azimuth angles to capture and exploit the abundance of multipath, conditioned upon using highly directional steerable antennas and beamforming algorithms at both the TX and RX.

Fig. 7 shows the distant-dependent lobe path loss for all lobes measured in Manhattan, at all measureable locations and angle orientations for both the TX and RX. The lobe path loss (LPL) was found with respect to a 5 m free space reference lobe, and a best-fit distant-dependent path loss model was used to determine the path loss exponent and shadowing factor. In Fig. 7, the measured lobe power was subtracted from the 5 m free space reference lobe total

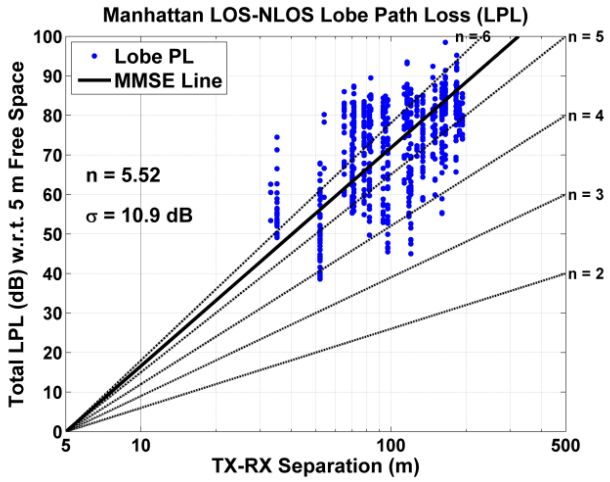

Fig. 7. Manhattan lobe path losses (LPL) with respect to a 5 m free space reference lobe as a function of TX-RX separation distance at 28 GHz. The solid black line is the MMSE best line fit through the lobe path losses. The theoretical maximum lobe power of the free space reference lobe at 5 m was subtracted from every total lobe power to recover the lobe path loss. The lobe path loss exponent is 5.52 and the shadow factor is 10.9 dB.

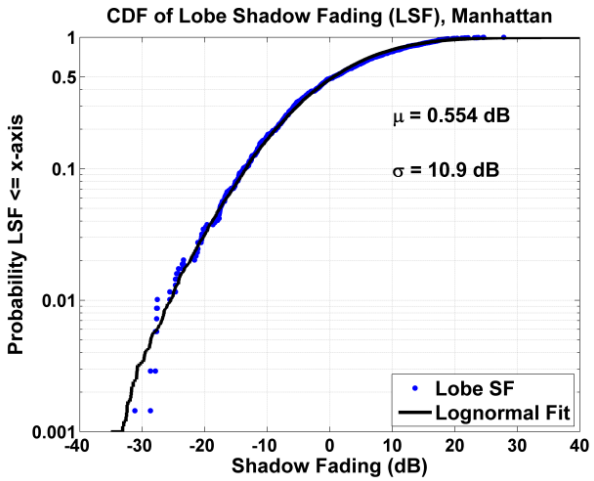

Fig. 8. Cumulative Distribution Function of the lobe shadow fading (blue dots) in Manhattan at 28 GHz. The average and standard deviation of the shadow fading are 0.5 dB and 10.9 dB, respectively. The shadow fading distribution follows a lognormal distribution (normal distribution with dB-values) (black solid line). Shadow fading at distance *d* is found by subtracting the MMSE lobe path loss from the actual lobe path loss.

power, thus recovering lobe path loss. The 5 m free space reference lobe is defined as the reference lobe that is measured (or found theoretically) when the TX and RX are on boresight to one another, with the RX in the Fraunhofer region. A free space reference lobe has well defined properties against which we can compare any measured lobe from New York City. The total lobe power is calculated by summing the received powers (in the linear scale) at every 10° angular increment across the reference lobe using a LOS threshold of 10 dB below boresight received power level. We found that the 5 m reference LAS was 20° since the 24.5 dBi RX antenna gain decreased by 10 dB at ±10° from boresight. The corresponding power

received on boresight (i.e. 0°) was added (in the linear scale) to the total power received at ±10°, and the total lobe power at 5 m free space was found to be 4.7 dBm with a maximum transmit power of 30 dBm. The received power in LOS and NLOS environments was observed to generally vary over 10 dB and 20 dB dynamic ranges, respectively, because the received multipath signals in a LOS environment arrive from most RX azimuth directions and are much stronger than multipath signals propagating in NLOS environments, in which energy arrives at just a few main directions of arrivals. The lobe path loss exponent was n = 5.52 using the MMSE method, and the shadow factor was σ = 10.9 dB. These values are similar to path loss exponents reported in [4]. The lobe path loss exponent is high because the reference lobe power is much stronger than any lobe power measured in Manhattan. The decay of lobe power over space (i.e. the energy propagating in a main spatial propagation route from the TX to the RX) decays significantly when comparing it to the 5 m free space reference lobe power.

Fig. 8 displays the cumulative distribution function (CDF) of the shadow fading in all Manhattan locations. The shadow fading was computed by taking the difference between all the measured lobe path loss values and the best-fit distant-dependent mean lobe path loss line of n = 5.52. The shadow fading fits well to a lognormal distribution (a normal distribution with dB-values), with a mean of 0.5 dB (close to zero mean) and a standard deviation of 10.9 dB.

V. Conclusion

This paper presented an investigation of AOA and AOD of wireless multipath propagation and small-scale fading effects at 28 GHz in New York City, using highly directional steerable antennas. It was found that small-scale fading is relatively negligible (± 2 dB about the mean power level) over a 10λ distance at fixed AOA using high gain antennas. A preliminary theory of lobes, necessary to predict AOA and AOD statistics in an urban micro-cellular environment such as New York City was developed. The lobe path loss exponent was found to be 5.52 with respect to a 5 m free space reference lobe, with a shadow factor of 10.9 dB. Shadow fading can be modeled by a lognormal random variable with mean 0.5 dB (close to zero mean) and standard deviation 10.9 dB. An average number of two to three main propagation routes (i.e. lobes) from TX to RX was discovered, and a new type of statistical modeling framework was proposed. These initial models will be used to create a 28 GHz SSCM, and will help cellular designers to build antenna arrays and beam steering algorithms in a way which will exploit the AOA and AOD statistics found in urban environments, by selecting the azimuth directions which maximize signal strength, thus improving signal quality and system capacity.

VI. Acknowledgement

This work was sponsored by Samsung DMC R&D Communications Research Team (CRT) through Samsung Telecommunications America, LLC. The authors wish to thank George MacCartney, Shuai Nie, and Junhong Zhang of NYU WIRELESS, as well as DuckDong Hwang and Shadi Abu-Surra of Samsung, the NYU administration, NYU Public Safety, and NYPD for their contribution to this project. Measurements recorded under U.S. FCC Experimental License 0040-EX-ML-2012.

References

[1] F. Gutierrez, S. Agarwal, K. Parrish, and T. S. Rappaport, "On-Chip Integrated Antenna Structures in CMOS for 60 GHz WPAN Systems," IEEE Journal on Selected Areas in Communications, vol. 27, no. 8, October 2009.

[2] T. S. Rappaport, J. N. Murdock, and F. Gutierrez, "State of the Art in 60-GHz Integrated Circuits and Systems for Wireless Communications," Proceedings of the IEEE, vol. 99, no. 8, pp. 1390–1436, August 2011.

[3] P. Zhouyue and F. Khan, "An Introduction to Millimeter Wave Mobile Broadband Systems," IEEE Communications Magazine, vol. 49, no. 6, pp. 101–107, June 2011.

[4] Y. Azar, G. N. Wong, K. Wang, R. Mayzus, J. K. Schulz, H. Zhao, F. Gutierrez, D. Hwang, and T. S. Rappaport, "28 GHz Propagation Measurements for Outdoor Cellular Communications Using Steerable Beam Antennas in New York City," 2013 IEEE International Conference on Communications (2013 ICC), June 9–13 2013, to appear.

[5] T. S. Rappaport and J. N. Murdock, "Power Efficiency and Consumption Factor Analysis in Broadband Millimeter Wave Cellular Networks," 2012 IEEE Global Communications Conference, December 3–7 2012.

[6] J. C. Liberti and T. S. Rappaport, "Analysis of CDMA Cellular Radio Systems Employing Adaptive Antennas in Multipath Environments," IEEE 46th Vehicular Technology Conference, 1996. Mobile Technology for the Human Race, vol. 2, pp. 1076–1080, 28 Apr–1 May 1996.

[7] G. Durgin and T. S. Rappaport, "Basic Relationship between Multipath Angular Spread and Narrowband Fading in Wireless Channels," IET Electronics Letters, vol. 34, no. 25, pp. 2431–2432, December 10 1998.

[8] Hao Xu; Kukshya, V.; Rappaport, T.S., "Spatial and Temporal Characteristics of 60-GHz Indoor Channels," Selected Areas in Communications, IEEE Journal on, vol.20, no. 3, pp. 620-630, Apr 2002.

[9] 3rd Generation Partnership Project, "Spatial Channel Model for Multiple Input Multiple Output (MIMO) Simulations," March 2011. http://www.3gpp.org/ftp/Specs/html-info/25996.htm

[10] International Telecommunication Union, "Guidelines for Evaluation of Radio Interface Technologies for IMT-Advanced," 2008. http://www.itu.int/pub/R-REP-M.2135-1-2009

[11] Seidel, S.Y.; Arnold, H.W., "Propagation Measurements at 28 GHz to Investigate the Performance of Local Multipoint Distribution Service (LMDS), "Global Telecommunications Conference, 1995. GLOBECOM '95., IEEE, vol.1, no., pp.754-757 vol.1, 14-16 Nov. 1995.

[12] T. S. Rappaport, E. Ben-Dor, and J. N. Murdock, "38 GHz and 60 GHz Angle Dependent Propagation for Cellular and Peer to Peer Wireless Communications," IEEE International Conference on Communications (2012 ICC), June 10–15 2012.